Dalton Transactions

Biomimetic Catalysts of Iron–based Metal-Organic Frameworks with High Peroxidase-Mimicking Activity for Colorimetric Biosensing

Journal:	*Dalton Transactions*
Manuscript ID	DT-ART-07-2020-002504.R3
Article Type:	Paper
Date Submitted by the Author:	11-Feb-2021
Complete List of Authors:	Wang, Xiao-Ning; Luoyang Normal University, Zhao, Yu-Meng; Huazhong Univ Sci Li, Jialuo; Texas A&M University, Chemistry Pang, Jiandong; Texas A&M University, Department of Chemistry Wang, Qiang; Wuhan Textile University Li, Bao; Huazhong Univ Sci , ; huazhong university of science and technology Zhou, Hong-Cai; Texas A&M University, Chemistry

Journal Name

ARTICLE

Biomimetic Catalysts of Iron–based Metal-Organic Frameworks with High Peroxidase-Mimicking Activity for Colorimetric Biosensing

Received 00th January 20xx,
Accepted 00th January 20xx

DOI: 10.1039/x0xx00000x

www.rsc.org/

Xiao-Ning Wang[a], Yumeng Zhao[b], Jia-Luo Li[c], Jian-Dong Pang[c], Qiang Wang[a] , Bao Li*[b] and Hong-Cai Zhou*[c]

Abstract: The field of Metal-Organic Frameworks (MOFs)-based biomimetic catalyst has achieved great progresses, but is still in its infancy stage. The systematic investigation on the tailored construction of MOF-based biomimetic catalysts is required for further development. Herein, two iron-based MOFs, $[(Fe_3O)_2(H_2O)_4(HCOO)(L)_2]_n$ (HUST-5: H_6L = hexakis(4-formylphenoxy) cyclotriphosphazene; HUST = Huazhong University of Science and Technology) and $[(Fe_3O)(H_2O)_3(L)]_n$ (HUST-7) had been fabricated through the assembly of the different iron clusters and hexa-carboxylate ligand under the control of the added acid species. Two MOFs exhibit the distinct secondary building units (SBUs) and topological structures, which could be played as the biomimetic catalysts for the systematic comparisons of the structural characteristics and catalytic activity. Both MOFs have possessed the catalytic activity similar to the natural peroxidases towards to catalyze the oxidation of a variety of substrates. Significantly, HUST-5 and HUST-7 can effectively catalyze the oxidation of 3,3',5,5'-tetramethylbenzidine (TMB) by H_2O_2 accompanied with a significant colorimetric biosensing. Although with the same compositions, the different catalytic performances had been presented due to the differences of porous structures and characteristics of SBUs in two Fe-MOFs, which had been also validated by theoretical calculation results. Furthermore, the phenomenon of colorimetric biosensing could be significantly suppressed by the addition of ascorbic acid (AA) during the oxidation process of TMB. Observed from these findings, a facile colorimetric biosensing platform for detecting H_2O_2 and ascorbic acid has been successfully explored. Therefore, this work provides another unique perspective for the tailor-made preparation of stable MOF-based peroxidase mimics with excellent catalytic performance and colorimetric biosensing.

Introduction

Natural enzymes are ubiquitous in nature, which could be of the highly selective catalysts for a wide range of vital reactions under mild conditions and facilitate to shorten synthetic routes that obviate the use of harsh reagents, which has been widely utilized in biotechnology, medicine, environmental analysis, food processing and biosensing. However, the wide applications of enzymes can be severely restricted by their intrinsic fatal defect such as low stability, easily inactive in harsh chemical environment, difficulties in separation from the reaction mixture and in the reuse of the enzyme.[1-4] Among the functionality assays, colorimetric biosensing has attracted great attention due to its specific advantages as low cost, simplicity, and practicality.[5-7] Versatile smart materials had been prepared in order to turn the detection phenomenon into colour changes. However, the lack of the systematic investigation of structural-activity relationship and mechanism had seriously hindered the development of the related field. Therefore, to address these issues, developing artificial materials as potential alternatives to mimic natural enzymes with high catalytic activity and selectivity and circumvent the above problems has been a sought-after goal in the future.

Metal–organic frameworks (MOFs) have attracted increasing attention due to their special and diverse porous structures and functional performances.[8] Recently, MOFs-based biomimetic enzymes or catalysts are gradually emerging, which has been validated by several Fe- and Ce-MOFs that exhibit the highly catalytic activity similar to natural peroxidases.[9-24] Moreover, MOFs-based photoresponsive oxidase mimics including those for colorimetric sensing have been developed, in which the dissolved oxygen is activated by light for oxidation of a series of substrates in the absence of H_2O_2.[25] The metal-oxide clusters within the nanostructure of MOFs could exhibit semiconductor properties, with organic linkers as antennae to harvest photons. Nevertheless, weak

[a] Hubei Key Laboratory of Biomass Fibers and Eco-dyeing & Finishing, College of Chemistry and Chemical Engineering, Wuhan Textile University, Wuhan, Hubei, 430073, PR China.

[b] Key laboratory of Material Chemistry for Energy Conversion and Storage, School of Chemistry and Chemical Engineering, Huazhong University of Science and Technology, Wuhan, Hubei, 430074, PR China. E-mail: libao@hust.edu.cn.

[c] Department of Chemistry, Texas A&M University, College Station, Texas 77843-3255, United States.

visible absorption by these metal-oxide clusters limits their applications. The presented results fully manifest the future prospects of MOF as biomimetic catalysts along with colorimetric biosensing behaviors. However, the specific research field is still in its infancy stage. The existing works only reported the different structures and corresponding catalytic performances, but it is difficult to systematically study the catalytic mechanism and outline the structure-activity relationship. How to effectively construct MOFs consisted of the same components but different topologies and systematically compare their catalytic activities and mechanisms should be the key to further promote the development of MOFs-based biomimetic sensing. Correspondingly, giving full play to the unique advantages of MOFs in structural regulation will help to achieve greater breakthroughs in the related field.

Herein, considering the above statements, the reaction system containing iron ions and hexakis(4-formylphenoxy) cyclotriphosphazene (H_6L, Scheme 1) was utilized based on the following considerations: both iron ion and cyclotriphosphazene have been proved to be of the biocompatible materials which are the prerequisites for biomimetic catalysts;[26-30] unlike to the rigid ligands utilized in the reported MOFs-based catalysts, the selected hexa-carboxyl linkers exhibits the semi-rigid configuration, which is very beneficial for constructing the different MOFs with the same compositions; the highly connection mode between Fe clusters and hexa-carboxyl ligands would work in synergy to fabricate the stable platforms for the application of heterogeneous catalysis. In accordance with our assumptions, two porous Fe-based frameworks, $[(Fe_3O)_2(H_2O)_4(HCOO)(L)_2]_n$ (HUST-5) and $[(Fe_3O)(H_2O)_3(L)]_n$ (HUST-7), which possess the different secondary building units (SBUs) and topological structures had been constructed by fine-tuning the species of the added acid. The high connection modes between Fe-clusters and hexa-carboxyl ligands endow these two MOFs with excellent chemical stability, and both MOFs have possessed the catalytic activity similar to the natural peroxidases towards to catalyze the oxidation of a variety of substrates accompanied with a significant colorimetric biosensing. The detailed comparison of crystal structures, topological frameworks, catalytic properties and theoretical calculation for the catalytic systems had been presented. Observed from these findings, this work provides another unique perspective for the tailor-made preparation of stable MOF-based peroxidase mimics with excellent catalytic performance and colorimetric biosensing.[31-33]

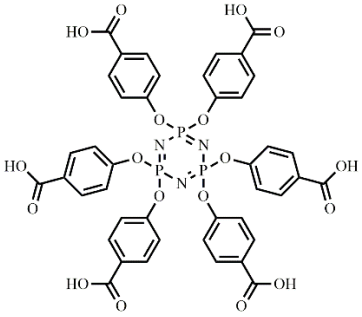

Scheme 1. The hexa-carboxyl linker H_6L used to construct HUST-5 and HUST-7.

Results and discussion

Crystal structure of two MOFs

HUST-5 had been introduced by our previous research work, which exhibits the excellent porous structure and chemical stability. Coupled with the decoration of iron clusters with open metal sites in the channels of framework, HUST-5 is suitable for promotion as one new functional material carrier. The original method for HUST-5 is complicated since the utilization of Fe_3O inorganic material. In order to enhance the product yield, the synthesis process had been optimized by changing the starting materials as $FeCl_2$ and hexa-carboxyl ligands. After adding the different species of acids as formic acid and acetic acid, two Fe-MOFs with the different SBUs, 3D porous frameworks and topologies had been constructed, which could be ascribed to the versatile synergistic effect between the iron-based clusters and ligands.

The basic compositions of HUST-5 is comprised of Fe_3O-COO-Fe_3O clusters and hexa-carboxyl linkers. Different to the other reported MOFs with $[Fe^{III}_2Fe^{II}O(COO)_6(H_2O)_3]$ cluster,[34-37] in HUST-5, two adjacent Fe_3O clusters are bridged by formate

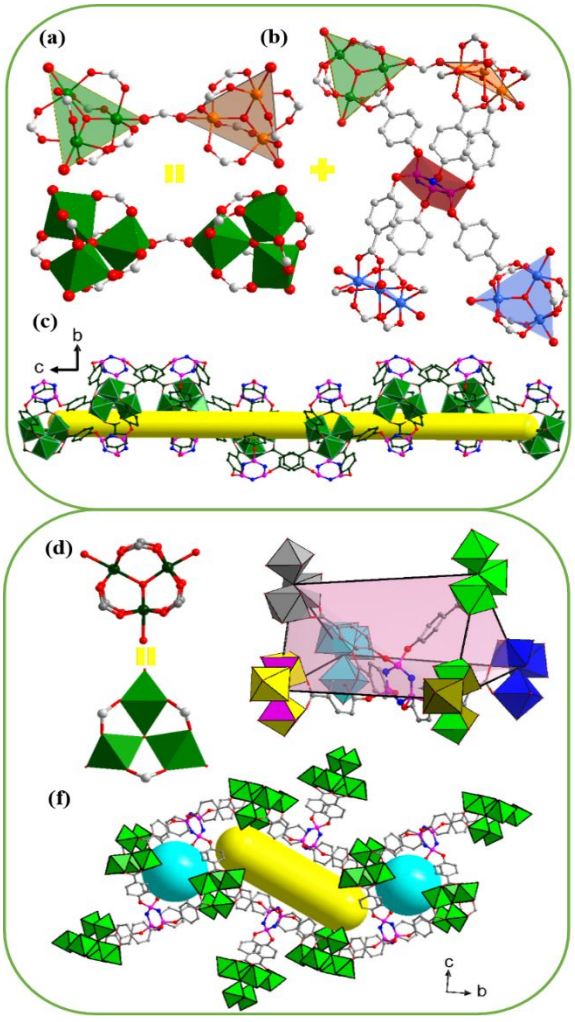

Figure 1. Crystal structures for HUST-5 (a-c) and HUST-7 (d-f). View of the conformation of hexa-nuclear cluster (Fe_3O-COO-Fe_3O) and tri-nuclear cluster (Fe_3O) (a, d). The coordination environment of hexa-carboxylate ligands (b, e). One dimensional SBU chain and two types of 1D channels along a-axial direction(c, f).

anion to form the novel hexa-nuclear cluster (Figure 1a). Two coordinated water molecules had been substituted by the bridged formate anion. Furthermore, the adjacent Fe_3O-COO-Fe_3O clusters are inter-linked by hexa-carboxyl ligands to form the intermittent chain, which is capped by four ligands to satisfy the saturate coordination environment of iron cluster (Figure 1c). Each 1D chain had been further surrounded by another four parallel chains to form the final 3D porous framework with a 64.2 % solvent-accessible void calculated by the *PLATON* routine (Figure 2a). The surface of channel had been decorated with open metal sites of iron-based clusters. Two types of hexa-carboxyl ligands had been stabilized in HUST-5, which bind three hexa-nuclear clusters. Due to the close distance of hexa-nuclear clusters, all of these hexa-carboxyl ligands adopt the approximate columnar configurations to inter-connect different one-dimensional chains with $C_{carboxyl}$-$O_{substituted}$-$P_{central}$ angles varied from 118.9 to 130.5°. The corresponding topological structure for HUST-5 had been calculated as *scu-3,6-C2221* with Schläfli symbol of $\{4\cdot6^2\}_2\{4^2\cdot6^9\cdot8^4\}$ by TOPOS 4.0 when the hexa-nuclear clusters and ligands had been simplified as 6- and 3-connected nodes (Figure 2b).

Under the similar reaction conditions except for the addition of acetate acid, a distinct framework, HUST-7 with rod shape, had been constructed. Structural characterization reveals that HUST-7 crystallizes in orthorhombic *P*bam space group, and consists of the typical tri-nuclear $[Fe^{III}_2Fe^{II}O(COO)_6(H_2O)_3]$ cluster (Figure 1d). Each tri-nuclear cluster had been further capped by six ligands, which itself binds six tri-nuclear iron clusters to form the final 3D porous structure (Figure 2c). The configuration of ligand could be seen as triangular prism along with the $C_{carboxyl}$-$O_{substituted}$-$P_{central}$ angles from 121.4 to 129.2° (Figure 1e). Two types of 1D channels along *a*-axial direction had been reserved in the final framework (Figure 1f), along with 60.8% of the total volume calculated by the *PLATON* routine. The corresponding topological structure for HUST-7 had been analyzed to be a 6-c *sni* net with Schläfli symbol of $\{4^{11}\cdot6^4\}$ as determined by TOPOS 4.0 (Figure 2d).Compared to the related results in HUST-5, the synergistic effect between the different types of SBUs and semi-rigid ligands must be responsible for the fabrication of distinct topological structures. The addition of formic acid facilitates the aggregation of tri-nuclear iron clusters, while the counter-part ligand must twist its configuration to stabilize the final three-dimensional framework. As a result, two different MOFs along with the different compositions, density of open metal sites, porous channels and topologies, had been finally presented just via the addition of different acid types. However, both of the two MOFs possess the stable porous structure decorated with open metal sites of SBUs, which endows the possibilities of these two MOFs as heterogeneous catalysts.

The thermal and chemical stability of HUST-5 and HUST-7 had been determined by thermogravimetric analysis (TGA, Figure S6) and PXRD measurements (Figure S7 and S8), illustrating the stable porous structure under different harsh conditions. Thermogravimetric analysis reveals that HUST-5 and HUST-7

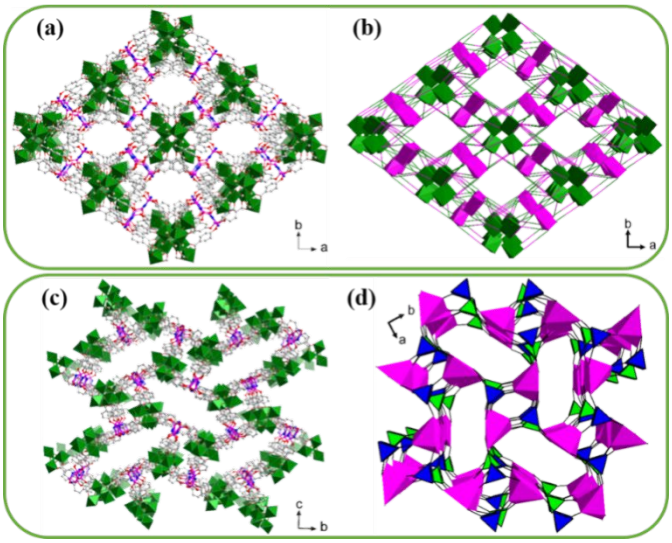

Figure 2. Partial view of 3D porous structure and topological structure for HUST-5 (a, b) and HUST-7 (c, d).

can be stable up to 300 °C. There is about 43% for HUST-5 and 67% for HUST-7 weight loss below 250 °C, which is due to the removal of DMF and water molecules. Moreover, the permanent porosity of HUST-5 and HUST-7 had been confirmed by N_2 adsorption isotherms measured at 77 K, which exhibit the reversible type-I isotherm (Figure 3). HUST-5 fabricated from $FeCl_2$ gives a BET (Brunauer–Emmett–Teller) surface area of 645.3 $m^2\ g^{-1}$ and Langmuir surface area of 958.2 $m^2\ g^{-1}$, while the calculated values of HUST-7 are 603.1 and 887.5 $m^2\ g^{-1}$, respectively, indicating the smaller porous framework of HUST-7 compared to HUST-5 that is consistent with the results of structural characteristics. Furthermore, compared to the corresponding N_2 adsorption results of HUST-5 synthesized from Fe_3O cluster, the observed values of HUST-5 ($FeCl_2$) are decreased, which is ascribed to the reducing defects in crystal samples. The utilization of free Fe^{2+} ions would increase the lability of ligands, coordinative reversibility between Fe^{2+} and ligands, and "error checking" during the self-assemble process, which is favor for reducing defects, enhancing crystalline quality and phase purity of the resulting crystal samples. Therefore, by the utilization of $FeCl_2$ salt not only increase the convenience of synthesis, but also enhance the whole quality of the resulting crystal samples.[38, 39]

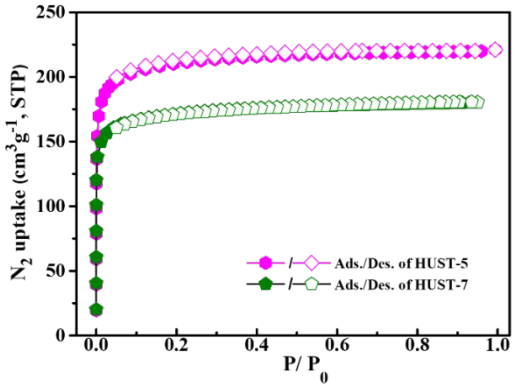

Figure 3. N_2 adsorption and desorption isotherms for HUST-5 and HUST-7 at 77 K.

Catalytic performances of two MOFs

To investigate the peroxidase-like activity, the catalytic oxidation of the peroxidase substrate 3,3',5,5'-tetramethylbenzidine (TMB) in the presence of H_2O_2 and heterogeneous catalysts as HUST-5 and HUST-7 had been explored. The detailed catalytic activity of Fe-MOFs for the reaction of TMB and H_2O_2 were evaluated by means of UV absorbance to monitor the oxidized product of TMB (oxTMB). As shown in Figure S9, only faint yellow solution and negligible absorption in the range 350 to 800 nm were observed in the absence of Fe-MOF. When HUST-5 or HUST-7 was introduced into the reaction systems containing H_2O_2 and TMB, the solution became green gradually, suggesting that Fe-MOFs could catalyze the oxidation TMB and produce the typical color reaction. UV–vis absorption tests showed that the green solution exhibits two intense characteristic absorbance at 369 and 660 nm, which is consistent with the previous results for the horseradish peroxidase enzyme.[40] The quick and obvious color-change behaviors clearly indicate that both Fe-MOFs exhibit the high peroxidase-like catalytic ability towards to the oxidation of TMB with the oxidant as H_2O_2. The heterogeneous catalyst firstly plays a peroxidase-mimicking role to decompose H_2O_2 into •OH radicals through electron transfer, which further react with TMB to generate a cation free radical TMB^{+}•. The apparent color change phenomenon should be ascribed to the origination of charge-transfer complex consisting of the states of TMB and TMB^{+}•.[41, 42] Apart from this, the authorized catalytic mechanism and the peroxidase-like activity of Fe-MOFs could be also consolidated by the obvious color change phenomenon during the oxidation of o-phenylenediamine (OPD) in the presence of H_2O_2.

In addition, the catalytic activity of these two MOFs is also dependent on the versatile environment conditions as pH values, temperature, catalyst concentration, and H_2O_2 concentration, similar to the behaviors for natural enzymes and other peroxidase mimetics. Therefore, the pH, temperature, catalyst concentration and H_2O_2 concentration dependent-activity of two Fe-MOFs have been also investigated in the current research. The optimal pH of HUST-5 and HUST-7 was approximately 4.0, which was very similar to that of natural enzyme HRP and other Fe-MOFs. After monitoring the catalytic performances with varying the temperature regions from 30 °C to 60 °C, the optimal catalytic temperature of HUST-5 and HUST-7 was 45 °C and 50 °C, respectively (Figure S10 and S14).

The steady-state kinetic assays were performed by varying one substrate concentration while keeping the other substrate concentration constant in the same catalytic assays. The obtained results indicate that the reaction process obeyed the typical enzymatic dynamic regulation of the Michaelis–Menten equation.[36] The kinetic parameters, such as the Michaelis–Menten constant (K_m) and maximum initial velocity (V_{max}), were obtained from a Lineweaver–Burk plot and are shown in Table S4. K_m is the Michaelis constant and is often associated with the affinity between substrate and catalyst. A low K_m means the strong affinity of the catalyst to the substrates.[43] For TMB oxidation reaction, the derived K_m value of 3.57 mM

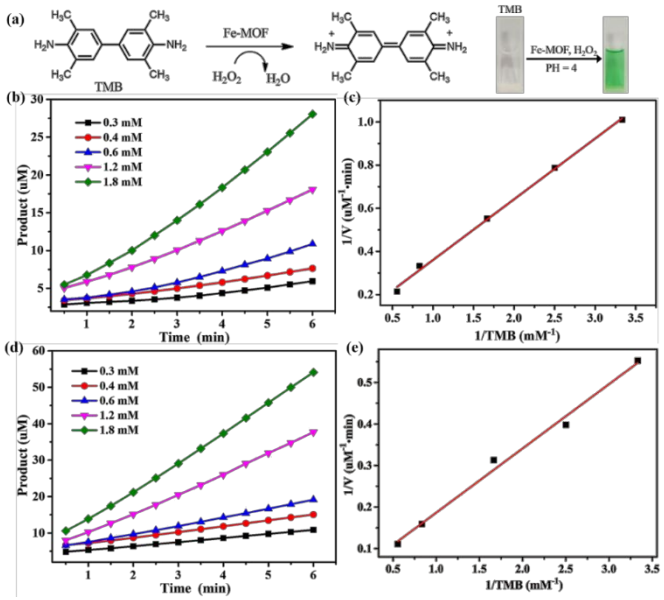

Figure 4. (a) Reaction schemes and images of peroxidase-like oxidation reaction of TMB catalyzed by Fe-MOF in NaAc buffer solution (pH = 4.0); The initial TMB oxidation profile catalyzed by HUST-5 (b) and HUST-7 (d), the concentrations of TMB range from 0.3 mM to 1.8 mM; Lineweaver-Burk plot of TMB oxidation catalyzed by HUST-5 (c) and HUST-7 (e).

for HUST-5 was lower than 4.9 mM for HUST-7, suggesting HUST-5 has a higher affinity for TMB than HUST-7. The higher density of catalytic centers in hexa-nuclear cluster of HUST-5 should be the origination of the different affinity compared to HUST-7. Additionally, the corresponding K_m values of HUST-5 and HUST-7 were significantly lower than the other peroxidase mimics (Table S4), indicating the stronger affinity than other mimics.

The high peroxidase-like activity of HUST-5 and HUST-7 had been also validated by the oxidation of o-phenylenediamine (OPD) peroxidase. As shown in Figure 5, under the similar catalytic conditions with the catalysts of two Fe-MOFs, OPD could be oxidized along with the obvious orange color. A Lineweaver–Burk plot with a nearly linear relationship can also be obtained (Figure 5c and 5e). The derived K_m values for HUST-5 and HUST-7 had been simulated as 1.18 mM and 1.72 mM, respectively, also indicating the strong affinity between

substrates and two Fe-MOFs and the same tendency observed in TMB systems. In term of the performances of these two catalytic systems, both of these two Fe-MOFs possess peroxidase-like activity towards the typical peroxidase substrates.

Detection of H_2O_2 and AA

Given that the TMB catalyzed by the peroxidase-mimicking Fe-MOFs, a direct detection of H_2O_2 via colorimetric sensing can be easily established based on the relationship between the concentration of H_2O_2 and the intensity of UV–vis absorbance at 660 nm. The intensities of the UV-vis absorption peaks at 660 nm increased with enhancing H_2O_2 concentration from 5 to 300 mM (Figure 6a and 6c). A linear relationship (Figure S13b and S17b) between the absorbance and the H_2O_2 concentration ranging from 5 to 50 μM for HUST-5 and HUST-7 (R^2 = 0.99 for HUST-5 and R^2 = 0.98 for HUST-7) was determined, with a detection limit of 1.84 μM and 4.26 μM, respectively, for HUST-5 and HUST-7 (Table S5). Furthermore, the resulting reaction solutions could induce a color variation which could be clearly seen by the naked eye, offering a convenient approach to detect H_2O_2 even at low concentrations.

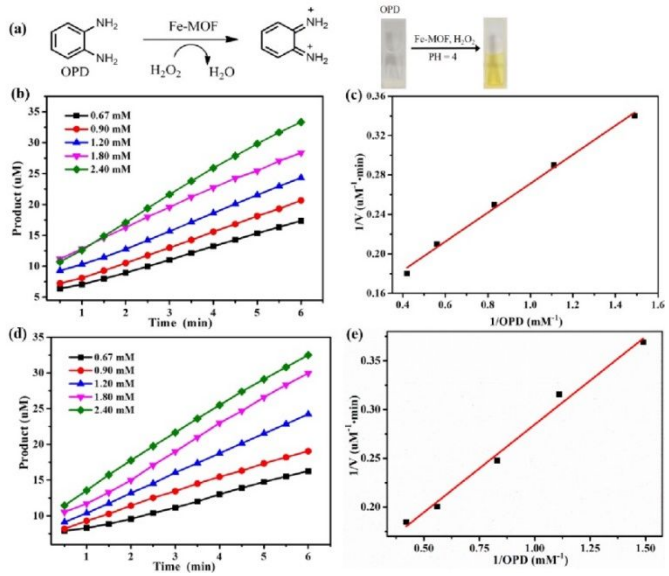

Figure 5. (a) Reaction schemes and images of peroxidase-like oxidation reaction of OPD catalyzed by Fe-MOF in NaAc buffer solution (pH = 4.0); The initial OPD oxidation profile catalyzed by HUST-5 (b) and HUST-7 (d), the concentrations of OPD range from 0.67 mM to 2.40 mM; (c) Lineweaver-Burk plot of OPD oxidation catalyzed by HUST-5 (c) and HUST-7 (e).

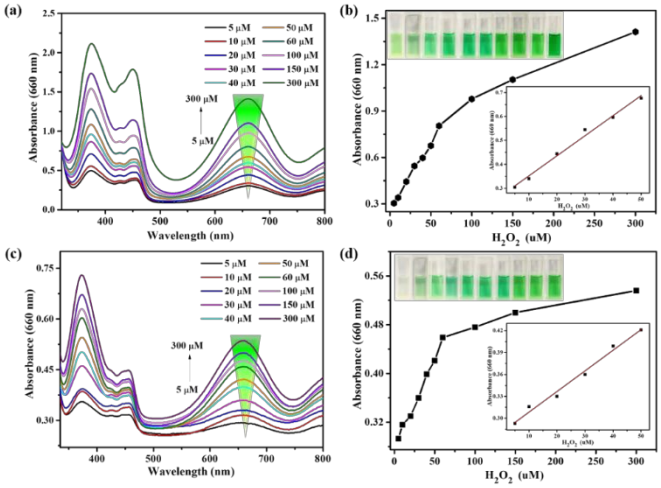

Figure 6. UV–vis absorbance spectra of TMB oxidation with various H_2O_2 concentrations (5-300 μM) using HUST-5 (a) and HUST-7 (c) as a peroxidase mimic; Dose–response curves for H_2O_2 detection in the range of 5-300 μM using HUST-5 (b) and HUST-7 (d) as a peroxidase mimic. Inset: corresponding linear calibration plots for H_2O_2 detection and the corresponding photographs for the formation of colored products with different concentrations of H_2O_2.

In addition, the TMB oxidation process can be effectively suppressed with the addition of a trace amount of ascorbic acid (AA), subsequently yielding a light green solution. In view of these observations, a colorimetric biosensor system for AA on the basis of HUST-5 and HUST-7 could be readily developed. As displayed in Figure 7a and 7c, the typical UV-vis absorption

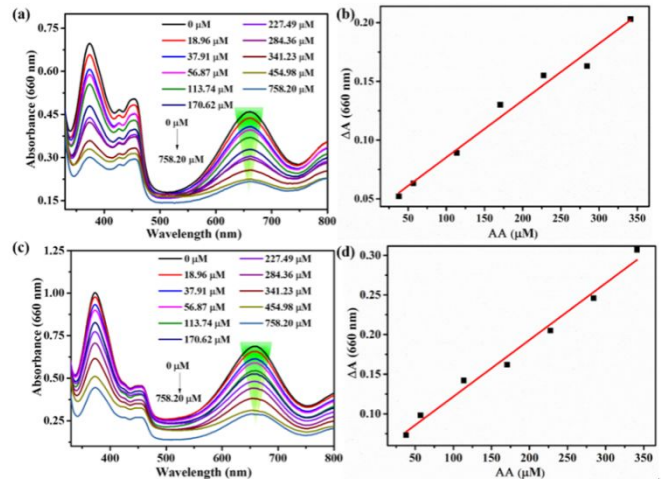

Figure 7. UV–vis spectra of TMB oxidation catalyzed by HUST-5 (a) and HUST-7 (c) in the presence of AA as an inhibitor in a pH = 4.0 NaAc buffer solution; The corresponding linear calibration plot for AA detection on the basis of HUST-5 (b) and HUST-7 (d). $\Delta A = A_0 - A_i$ (A_0 is the initial absorbance intensity at 660 nm without AA and A_i is the absorbance intensity at 661 nm with an AA concentration of i).

intensity at 660 nm decreased with an increase of AA concentration from 18.96–758.2 μM. The linear relationship between the ΔA ($\Delta A = A_0 - A_i$, A_0 is the initial absorbance intensity at 660 nm without AA and A_i is the absorbance intensity at 661 nm with an AA concentration of i) and the AA concentration in the range of 37.91–341.23 μM is estimated (R^2 = 0.99 for HUST-5 and R^2 = 0.98 for HUST-7) (Figure 7b and

7d). Based on S/N = 3, the detection limit is estimated to be 12.11 μM and 15.92 μM, respectively, for HUST-5 and HUST-7, which is comparable or even better than those of previously reported MOF-based peroxidase mimics in Table S5.

Theoretical calculation for catalytic mechanism

Due to the experimental limitations during catalytic process, the detailed mechanism could not be explored clearly. Normally, the mechanism had been presumed to be the ability of iron clusters to generate free hydroxyl radicals. However, the related interactions between iron-based catalysts and substrates had been not adequately considered, which might be ascribed to the lack of the proper platforms to carry out the systematic investigations. Herein, thanks to the explored structures and excellent catalytic properties, the interactions between iron-based catalysts and corresponding substrates had been investigated via theoretical calculation. Spin polarized Density functional theory calculations had been utilized to identify adsorption property of substrates onto iron-based catalysts by PBE/DNP theoretical level in the DMol^3 software.[44-46] Owing to the restrictions of huge computational cost and theoretical method, the simulation of the whole frameworks for these two MOFs were very difficult. Therefore, the related iron clusters along with their coordination environments had been isolated to set up the computational models, which should play the main role of catalytic active centers in catalytic reactions.

The simplified models had included the metallic centers and corresponding porous traits, which would provide the systematic investigations into the detailed catalytic mechanisms. Essentially, the nature of open metal sites plays the important role in determining the catalytic performances, which was usually fabricated via removing coordinated molecules. Herein, for two iron-based MOFs, the unsaturated coordination sites with Lewis acid had been formed via removing aqua molecules, and the corresponding dissociation energy had been calculated as 40.43 kcal/mol for HUST-7 and 27.80 kcal/mol for HUST-5. The small values illustrated the facile tendency for fabricating the desired open metal sites, and endow these two iron-based MOFs with potential as the effective catalysts. Furthermore, as shown in Figure 8, the composed structures after the adsorption of two substrates had been presented. The related substrates had been absorbed onto the frameworks via Fe···N or Fe···O interactions, along with the distances from 2.19 to 2.36 Å for HUST-7, and 2.28 to 2.34 Å for HUST-5. For HUST-7, the adsorption energy had been calculated as -2.34 eV for TMB and -2.25 eV for OPD, while the related values are -2.41 eV and -1.88 eV for HUST-5. These calculated values illustrate the strong interactions between these frameworks and substrates, which might be the reasons for the presented catalytic performances for two MOFs. The close interaction distances and adsorption energies for these two MOFs are also inconsistent with their similar catalytic performances. Furthermore, the strong overlap of 3d orbitals of iron centers in MOFs and 2p orbitals of O/N in substrates could also illustrate the mechanism of the efficient performances in oxidation reaction with the utilization of these two iron-based MOFs (Figure 9). Therefore, in term of the theoretical calculations, the easy formation of open metal sites, proper steric effect and strong interactions between metal centers and substrates should be the key factors for the desired heterogeneous catalysts, which had been presented by these two MOFs. Compared with HUST-7, HUST-5 has a slightly superior performance, which may be due to the higher density of iron clusters in the active hexa-nuclear center compared to the trinuclear center. Additionally, the different porous traits of these frameworks should be responsible for the slight differences in dynamic parameters.

On the basis of the above investigations, the biomimetic catalytic activities of two stable Fe-MOFs with the same compositions but different topologies had been systematically investigated. The excellent catalytic performances of HUST-5 and HUST-7 should be attributed to the controllable construction of stable 3D structures with biocompatibility

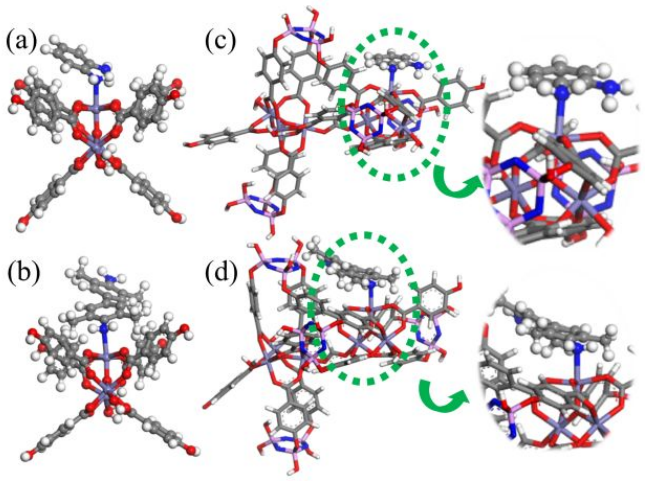

Figure 8. The calculated adsorption structures composed of the simplified frameworks and substrates: OPD and TMB for HUST-7 (a, b); OPD and TMB for HUST-5 (c, d).

Journal Name

ARTICLE

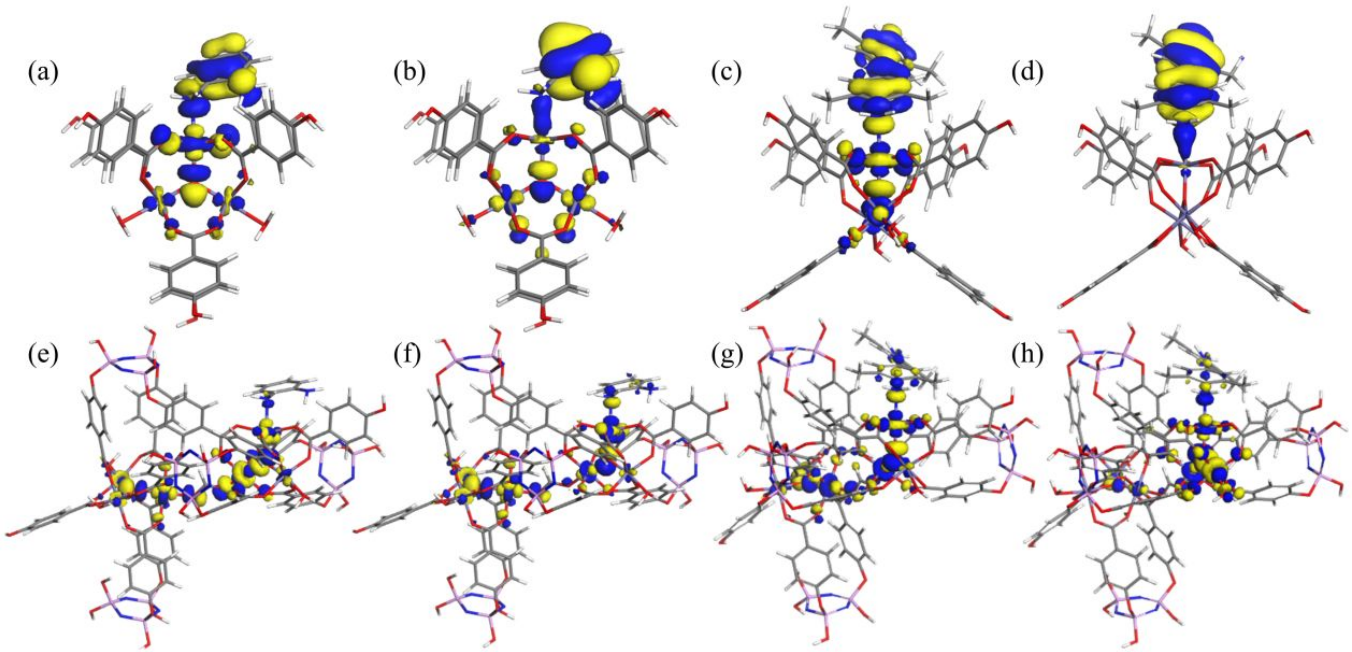

Figure 9. Frontier molecular orbitals for HUST-7 interacted with OPD (HOMO (a), HOMO-3 (b)) and TMB (HOMO (c), HOMO-2 (d)); Frontier molecular orbitals for HUST-5 interacted with OPD (HOMO (e), HOMO-1 (f)) and TMB (HOMO (g), HOMO-1 (h)).

components, large open channels and accessible catalytic sites for the substrates, which effectively facilitates the affinity between catalyst and substrates. Moreover, two MOFs with the same compositions exhibit the different catalytic performances, mainly due to their differences in the structural characteristics. Compared to the trinuclear cluster and irregular pores in HUST-7, the hexa-nuclear cluster, regular channels and higher density of catalytic centers of HUST-5 must be responsible for the differences. Overall, a comprehensive investigation of biomimetic catalytic properties of MOFs-based catalysts had been presented, suggesting a bright future on building MOF-based platforms for varieties of enzymatic mimics catalysis.

Conclusions

In summary, two water-stable Fe(III)-based MOFs, which exhibit intrinsic peroxidase-like activities, catalyzing the oxidation of 3,3',5,5'-tetramethylbenzidine (TMB) and o-phenylenediamine (OPD) when H_2O_2 serves as oxidant, have been constructed and characterized. Their catalytic performance is strongly relies on pH value, temperature, catalyst dosage and H_2O_2 concentration. Compared with natural enzymes, HUST-5 and HUST-7 as peroxidase mimic possess advantages of low-cost, easy preparation and storage, more stable to biodegradation, and less vulnerable to denaturation. Both Fe-MOFs oxidized TMB in a slightly acidic solution at pH 4.0 to produce color reaction in the presence of H_2O_2, which illustrate their great potential application as colorimetric sensor for H_2O_2 assay. Interestingly, antioxidants AA decreased the color intensity of the solution, which were indirectly determined by absorbance difference. In light of the fact that AA has a significant inhibition effect on the catalytic activity of Fe-MOFs, a simple colorimetric biosensing for AA was also successfully explored. We believed that the presented results could provide the possibility of building MOF-based platforms as enzymatic mimics catalysis and facilitate their utilization in immunoassays and biotechnology

Conflicts of interest

There are no conflicts to declare.

Acknowledgements

This work was supported by the financial supports of National Science Foundation of China (21971078, 21471062), the Center for Gas Separations Relevant to Clean Energy

Technologies, an Energy Frontier Research Center (EFRC) funded by the U.S. Department of Energy (DOE), Office of Science, and Office of Basic Energy Sciences (DESC0001015), Office of Fossil Energy, the National Energy Technology Laboratory (DE-FE0026472), and the Robert A. Welch Foundation through a Welch Endowed Chair to HJZ (A-0030), the Fundamental Research Funds for the Central Universities (2019kfyRCPY071, 2019kfyXKJC009). We gratefully acknowledge the Analytical and Testing Center, Huazhong University of Science and Technology, for analysis and spectral measurements. We also thank the staffs from BL17B beamline of the National Center for Protein Sciences Shanghai (NCPSS) at Shanghai Synchrotron Radiation Facility, for assistance during data collection.

Notes and references

1 I. Nath, J. Chakraborty and F. Verpoort, *Chem. Soc. Rev.*, 2016, **45**, 4127-4170;
2 E. Shoji and M. S. Freund, *J. Am. Chem. Soc.,* 2002, **124**, 12486-12493.
3 G. Wulff, *Chem. Rev.,* 2002, **102**, 1-28.
4 Y. Lin, J. Ren and X. Qu, *Acc. Chem. Res.,* 2014, **47**, 1097-1105.
5 J. Liu and Y. Lu, *Angew. Chem. Int. Ed.,* 2006, **45**, 90-94.
6 L. Su, J. Feng, X. Zhou, C. Ren, H. Li and X. Chen, *Anal. Chem.,* 2012, **84**, 5753-5758.
7 Y. L. Dong, H. G. Zhang, Z. U. Rahman, L. Su, X. J. Chen, J. Hu and X. G. Chen, *Nanoscale* 2012, **4**, 3969-3976.
8 Z. Lin, J. Lü, M. Hong and R. Cao, *Chem. Soc. Rev.,* 2014, **43**, 5867-5895.
9 F. Qin, S. Jia, F. Wang, S. Wu, J. Song and Y. Liu, *Catal. Sci. Technol.,* 2013, **3**, 2761-2768.
10 Z.-Y. Gu, J. Park, A. Raiff, Z. Wei and H.-C. Zhou, *ChemCatChem.,* 2014, **6**, 67-75.
11 M. Giménez-Marqués, T. Hidalgo, C. Serre and P. Horcajada, *Coord. Chem. Rev.,* 2016, **307**, 342-360.
12 E. Gkaniatsou, C. Sicard, R. Ricoux, J.-P. Mahy, N. Steunou and C. Serre, *Mater. Horiz.,* 2017, **4**, 55-63.
13 M. Xu, S. Yuan, X.-Y. Chen, Y.-J. Chang, G. Day, Z.-Y. Gu and H.-C. Zhou, *J. Am. Chem. Soc.,* 2017, **139**, 8312-8319.
14 Y. Wang, Y. Zhu, A. Binyam, M. Liu, Y. Wu and F. Li, *Biosens. Bioelectron.,* 2016, **86**, 432-438.
15 Z. Qi, L. Wang; Q. You and Y. Chen, *Biosens. Bioelectron.,* 2017, **96**, 227-232.
16 M. SK, S. Banesh, V. Trivedi and S. Biswas, *Inorg. Chem.,* 2018, **57**, 14574-14581.
17 H. Zheng, C. Liu, X. Zeng, J. Chen, J. Lü, R. Lin, R. Cao, Z. Lin and J. Su, *Inorg. Chem.,* 2018, **57**, 9096-9104.
18 D. Feng, Z. Gu, J. Li, H. Jiang, Z. Wei and H. Zhou, *Angew. Chem. Int. Ed.,* 2012, **51**, 10307-10310.
19 L. Ai, L. Li, C. Zhang, J. Fu and J. Jiang, *Chem. -Eur. J.,* 2013, **19**, 15105-15108.
20 Z. Jiang, Y. Liu, X. Hu and Y. Li, *Anal. Methods* 2014, **6**, 5647-5651.
21 J. Zhang, H. Zhang, Z. Du, X. Wang, S. Yu and H. Jiang, *Chem. Commun.,* 2014, **50**, 1092-1094.
22 Y. Xiong, S. Chen, F. Ye, L. Su, C. Zhang, S. Shen, S. Zhao, *Chem. Commun.* **2015**, *51*, 4635-4638;
23 R. Dalapati, B. Sakthivel, M. K. Ghosalya, A. Dhakshinamoorthy and S. Biswas, *CrystEngComm*., 2017, **19**, 5915-5925.
24 N. A. Dare, L. Brammer, S. A. Bourne and T. J. Egan, *Inorg. Chem.,* 2018, **57**, 1171-1183.
25 Z. M. Hua, X. Jiang, F.J. Xu, J. Jia, Z. Long and X. D. Hou, *Talanta*, 2016, **158**, 276-282.
26 X.-Q. Zhang, S.-W. Gong, Y. Zhang, T. Yang, C.-Y. Wang and N. Gu, *J. Mater. Chem.,* 2010, **20**, 5110-5116.
27 S. Liu, J. Tian, L. Wang, Y. Luo, G. Chang and X. Sun, *Analyst* 2011, **136**, 4894-4897.
28 W. He, H. Jia, X. Li, Y. Lei, J. Li, H. Zhao, L. Mi, L. Zhang and Z. Zheng, *Nanoscale* 2012, **4**, 3501-3506.
29 E. W. Ainscough, A. M. Brodie, A. B. Chaplin, J. M. O'Connor and C. A. Otter, *Dalton Trans.,* 2006, **10**, 1264-1266.
30 L. Wang, Y.-X. Yang, X. Y. Shi, S. Mignani, A. -M. Caminade and J.-P. Majoral, *J. Mater. Chem. B,* 2018, **6**, 884-895.
31 J. R. Bour, A. M. Wright, X. He and M. Dincă, *Chem. Sci.,* 2020, **11**, 1728-1737.
32 T. A. Fernandes, C. I. M. Santos, V. André, J. Kłak, M. V. Kirillova and A. M. Kirillov, *Inorg. Chem.,* 2016, **55**, 125-135.
33 A. M. Kirillov, J. A. S. Coelho, M. V. Kirillova, M. F. C. Guedes da Silva, D. S. Nesterov, K. R. Gruenwald, M. Haukka, and A. J. L. Pombeiro, *Inorg. Chem.,* 2010, **49**, 6390-6392.
34 H. Chevreau, T. Devic, F. Salles, G. Maurin, N. Stock and C. Serre, *Angew. Chem. Int. Ed.,* 2013, **52**, 5056-5060.
35 K. Wang, D. Feng, T. Liu, J. Su, S. Yuan, Y. Chen, M. Bosch, X. Zou and H. Zhou, *J. Am. Chem. Soc.,* 2014**, 136**, 13983-13986.
36 J. Park, D. Feng and H. Zhou, *J. Am. Chem. Soc.,* 2015**, 137**, 1663-1672.
37 J. Wang, Y. Zhang, M. Li, S. Yan, D. Li and X. Zhang, *Angew. Chem. Int. Ed.,* 2017**, 56**, 6478-6482.
38 K. Guesh, C. A. D. Caiuby, Á. Mayoral, M. Díaz-García, I. Díaz and M. Sanchez-Sanchez, *Cryst. Growth Des.,* 2017, **17**, 1806-1813.
39 D. Bara, C. Wilson, M. Mörtel, M. M. Khusniyarov, S. Ling, B. Slater, S. Sproules and R. S. Forgan, *J. Am. Chem. Soc.,* 2019, **141**, 8346-8357.
40 L. Z. Gao, J. Zhuang, L. Nie, J. B. Zhang, Y. Zhang, N. Gu, T. H. Wang, J. Feng, D. L. Yang, S. Perrett and X. Y. Yan, *Nat. Nanotechnol.,* 2007, **2**, 577-583.
41 Y. Chen, H. Cao, W. Shi, H. Liu and Y. Huang, *Chem. Commun.,* 2013, **49**, 5013–5015.
42 X. Sun, S. Guo, C.-S. Chung, W. Zhu and S. Sun, *Adv. Mater.,* 2013, **25**, 132-136.
43 A. K. Dutta, S. Das, S. Samanta, P. K. Samanta, B. Adhikary and P. Biswas, *Talanta,* 2013, **107**, 361-367.
44 B. Delley, *J. Chem. Phys*., 1990, **92**, 508-517.
45 B. Delley, *J. Chem. Phys*., 1991, **94**, 7245-7250.
46 B. Delley, *J. Chem. Phys*., 2000, **113**, 7756-7764.

